ADVANCING EARTH AND SPACE SCIENCES

Geophysical Research Letters

RESEARCH LETTER

10.1029/2023GL104375

Key Points:

- Seismicity in the Ridgecrest area is modulated by the solid Earth tides
- Peak seismicity occurs when tidal Coulomb stress or stress rate favors rupture
- Strength of tidal triggering is gradually increasing in the rupture area about 2 years before the M_w 7.1 2019 mainshock

Supporting Information:

Supporting Information may be found in the online version of this article.

Correspondence to:

E. Beaucé,
ebeauce@ldeo.columbia.edu

Citation:

Beaucé, E., Poli, P., Waldhauser, F., Holtzman, B., & Scholz, C. (2023). Enhanced tidal sensitivity of seismicity before the 2019 magnitude 7.1 Ridgecrest, California earthquake. *Geophysical Research Letters*, *50*, e2023GL104375. https://doi.org/10.1029/2023GL104375

Received 1 MAY 2023
Accepted 8 JUL 2023

Author Contributions:

Conceptualization: Eric Beaucé, Piero Poli, Felix Waldhauser, Benjamin Holtzman, Christopher Scholz
Formal analysis: Eric Beaucé
Investigation: Eric Beaucé
Methodology: Eric Beaucé, Piero Poli
Software: Eric Beaucé
Writing – original draft: Eric Beaucé

Enhanced Tidal Sensitivity of Seismicity Before the 2019 Magnitude 7.1 Ridgecrest, California Earthquake

Eric Beaucé[1], Piero Poli[2], Felix Waldhauser[1], Benjamin Holtzman[1], and Christopher Scholz[1]

[1]Lamont-Doherty Earth Observatory, Columbia University, New York, NY, USA, [2]Dipartimento di Geoscienze, Università di Padova, Padova, Italy

Abstract Earth's crust is continuously subjected to oscillatory stress perturbations due to the solid Earth and ocean tides. The seismic response to such stress modulations carries information on earthquake physics and crustal properties. Experimental and observational studies suggested but could not demonstrate that the strength of tidal modulation of seismicity increases before large earthquakes. We tested this hypothesis by (a) developing a new, comprehensive 10-year long earthquake catalog preceding the 6 July 2019 magnitude 7.1 Ridgecrest, CA earthquake, and (b) applied our novel method for extracting a statistical signal of tidal modulation. Our results show enhanced tidal sensitivity of seismicity along the fault starting about 1.5 years before the mainshock, corroborating the hypothesis. This observation suggests that small magnitude earthquakes may be used to gain insight into subtle changes in fault conditions, bringing new promise for studying the earthquake preparation process.

Plain Language Summary The solid Earth experiences tides, like the ocean, it deforms under the gravitational attraction of the Sun and Moon. This deformation induces an oscillatory stress change in the crust with small peak-to-peak amplitudes of the order of 1 kPa (about 1% of the atmospheric pressure). Tidal stresses weakly influence the rate of earthquake occurrence and the characteristics of this modulation carry information on earthquake physics and crustal properties. On the basis of experimental and field observation studies, it has been proposed that the modulation of seismicity by the tides increases before a large earthquake. We tested this hypothesis by analyzing 10 years of seismicity before the *M*7.1 2019 Ridgecrest, CA earthquake. We first built a new, comprehensive earthquake catalog with our automated method and used our novel method to extract the signal of tidal modulation throughout the study period. We found that seismicity became strongly modulated by the tides about 2 years before the mainshock, thus corroborating the hypothesis.

1. Introduction

The search for a correlation between the solid Earth and ocean tides and the rate of seismicity is more than a century old (Schuster, 1897). In the late 20th century, several studies found no statistically meaningful correlation (e.g., Heaton, 1982; Rydelek et al., 1992; Vidale et al., 1998) but more recent studies (Cochran et al., 2004; Delorey & Chen, 2022; Métivier et al., 2009; Scholz et al., 2019) have presented strong evidence for the tidal modulation of seismicity. Studying the modulation of seismicity by the tides gives insights into fundamental earthquake physics like the earthquake nucleation process (Beeler & Lockner, 2003). It has been proposed that the temporal variations in the tidal modulation of a particular fault system's seismicity may inform us about its state (Chanard et al., 2019; Tanaka, 2010, 2012). Observations along mega thrusts (Tanaka, 2010, 2012) have led to the hypothesis that tidal modulation becomes stronger before a large rupture, but difficulties in objectively extracting statistically subtle signals from available data have prevented further demonstrations of such patterns (Wang & Shearer, 2015). This hypothesized pattern has been demonstrated in laboratory experiments (Chanard et al., 2019), but scaling to Earth conditions remains unclear. Because of the high societal and scientific implications of this hypothesis, understanding the underlying physics is crucial. In this study, we have developed a novel, assumption-free and data-driven method that allows to objectively extract the statistical signal of tidal modulation and test the hypothesis of increased modulation of microseismicity before large earthquakes.

The tidal modulation of seismicity is weak (Beeler & Lockner, 2003; Chanard et al., 2019; Pétrélis et al., 2021) and obscured by the many mechanisms driving seismicity (e.g., long-term tectonic forcing, slow slip events, earthquake interactions). In order to successfully characterize tidal modulation, tidal analysis must employ low magnitude of completeness catalogs (Vidale et al., 1998) and find new ways of extracting the tidal signal from

10.1029/2023GL104375

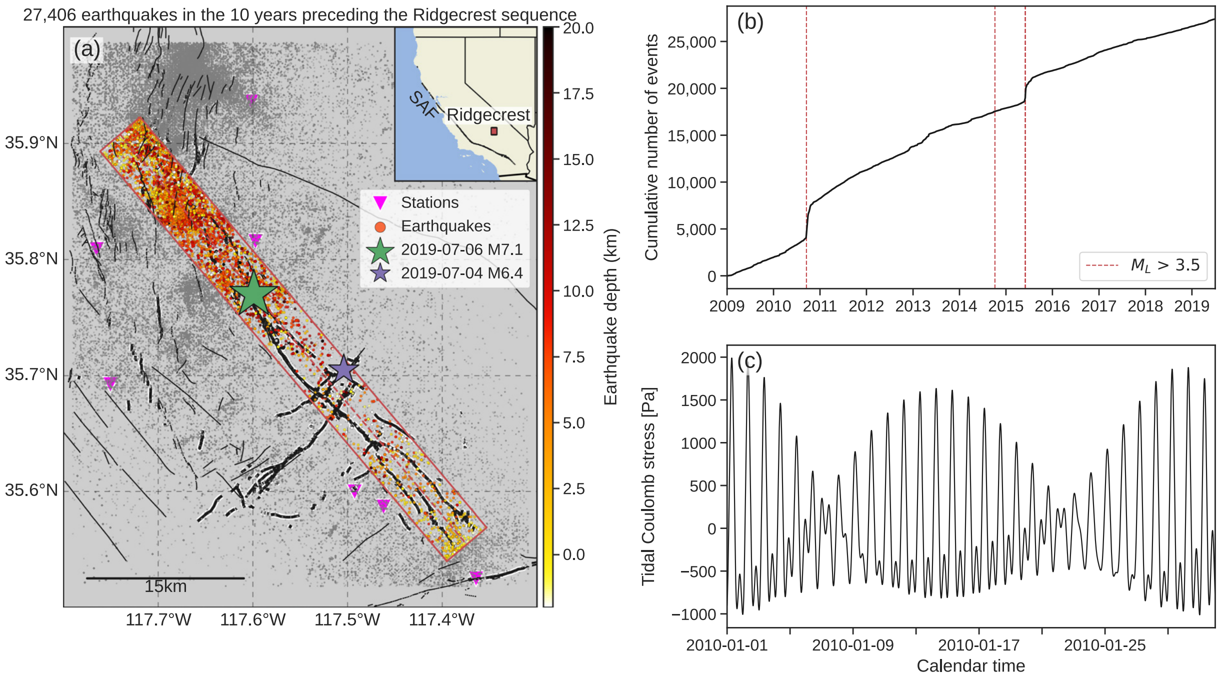

Figure 1. (a) Locations of the 191,569 detected earthquakes between 1 January 2009 and 3 July 2019; 27,406 earthquakes are located in the box of interest (5 km wide, red box). Depths are color-coded only for earthquakes within the box and with a horizontal location uncertainty less than 5 km. (b) Cumulative number of earthquakes within the box as a function of time. The timings of the $M_L > 3.5$ events are shown with the red dashed vertical bars. (c) One month of tidal Coulomb stress on a fault that is optimally oriented in the regional stress field.

the catalogs. Here, we address these requirements by taking advantage of recent advances in earthquake detection techniques that have greatly improved our ability to retrieve more and smaller events than is available in existing catalogs (Beaucé et al., 2022a; Mousavi et al., 2020; Zhu & Beroza, 2019) and using our new method to extract the signal of tidal modulation.

We analyzed the 10 years of continuous seismic waveforms preceding the 2019 Ridgecrest, CA earthquake sequence which started with a magnitude (M_w) 6.4 foreshock on 4 July 2019 and was followed, 34 hr later, by the M_w 7.1 mainshock. We built a new, comprehensive catalog from 1 January 2009 to 3 July 2019 (see Figure 1) using a fully automated, machine learning- and template matching-based earthquake detection and location method (Beaucé et al., 2022a). We detected 191,569 earthquakes with a magnitude of completeness of $M_c = -0.14$ (local magnitude), which is 44 times more events than in the Southern California Seismological Network (SCSN) catalog that has $M_c = 0.69$ (see Data Availability Statement). We used the SPOTL software (Agnew, 2012) to compute the strain due to the solid Earth and ocean tides, and stress was computed assuming typical crustal elastic moduli values (Tan et al., 2019). The tidal stress was decomposed into normal T_n and shear T_s stress on the optimally oriented fault based on the regional stress state as inferred from the focal mechanisms given in Yang et al. (2012) (and see Data Availability Statement) with the inversion method described in Beaucé et al. (2022b) (see Figure S1 in Supporting Information S1). We found that variations in tectonic stress across the study region are small (Figure S1 in Supporting Information S1) and therefore chose to work with the regional stress, which also simplified the subsequent tidal analysis. Normal and shear components were assembled to compute Coulomb stress, $\sigma = T_s + \mu T_n$, with a coefficient of friction $\mu = 0.6$ (see Figure 1c).

2. Quantifying the Strength of the Tidal Modulation

To estimate the strength of the tidal modulation of seismicity, we study the distribution of the seismicity rate as a function of the instantaneous phase ϕ of the tidal Coulomb stress, $\rho_{eq}(\phi)$, and of its amplitude σ, $\rho_{eq}(\sigma)$ (Cochran et al., 2004; Delorey et al., 2017; Scholz et al., 2019; Vidale et al., 1998) (see Figure 2). We compare these distributions to reference distributions, $\rho_{ref}(\phi)$ and $\rho_{ref}(\sigma)$, computed over the same period as $\rho_{eq}(\phi)$ and $\rho_{eq}(\sigma)$, that are proportional to the amount of time spent in each phase or stress bin and thereby represent the expected fraction

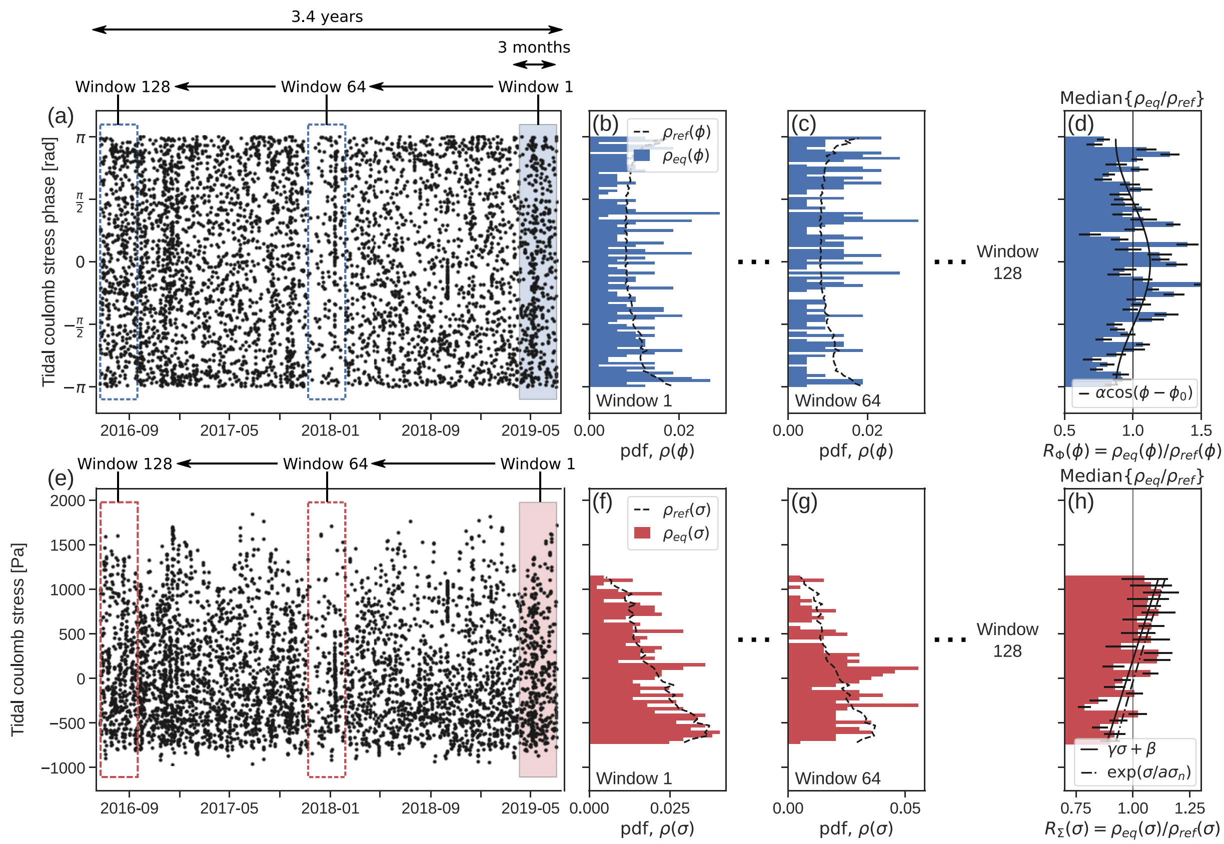

Figure 2. (a) Tidal Coulomb phase at the earthquake timings (0 rad is a local stress maximum). The 3.4-year window contains 128 3-month-long windows with 90% overlap. (b, c) Fraction of earthquakes in phase bins, $\rho_{eq}(\phi)$ (histogram), and reference distribution characterizing a tide-independent seismicity, $\rho_{ref}(\phi)$ (black dashed line), shown for two different 3-month windows. Note that $\rho_{ref}(\phi)$ is not a flat line because some phase bins cover a larger amount of time due to the non-sinusoidal shape of the tidal stress (see Figure 1c). The statistic of interest for tidal triggering is the ratio $R_\Phi(\phi) = \rho_{eq}(\phi)/\rho_{ref}(\phi)$. (d) Median ratio across all 128 3-month windows. Deviations from 1 indicate tidal modulation of the seismicity rate. The errors bars (black lines) are the dispersion in each bin. The median ratio is fitted with a periodic function. Panels (e–h) same as panels (a–d) but for Coulomb stress instead of phase. In (h), the median ratio $R_\Sigma(\sigma)$ is fitted with a linear function and the rate-and-state formula (see text). Note: Here, ϕ and σ are the instantaneous phase and amplitude of tidal Coulomb stress, but the same approach is applicable for any quantity of interest, namely: tidal shear and normal stress, as well as volumetric strain.

of earthquakes for a tide-independent seismicity. We analyze the ratios $R = \rho_{eq}/\rho_{ref}$ to determine whether the observed seismicity rate is significantly modulated by the tides. These ratios are similar to the excess number of earthquakes used in some studies (Cochran et al., 2004; Thomas et al., 2012). To gain insights into which stress component modulates seismicity, we follow an identical procedure to study the distribution of seismicity as a function of the instantaneous phase of the tidal shear and normal stresses and tidal volumetric strain.

The temporal clustering of earthquakes, for example, during aftershock sequences, can introduce considerable bias in ρ_{eq} by populating some bins with many events. We mitigate this bias and that introduced by other transient phenomena by repeatedly computing the ratios in 128 3-month-long, 90% overlapping sliding windows and taking the median across all windows as our final estimate of R (see Figure 2). One estimate of R thus senses a 3.4-year time period. The benefits of our tidal analysis method are two-fold: it accounts for the full complexity of the tidal stress time series by considering the stress instantaneous phase and amplitude, and it addresses the problem of temporal clustering without removing subjectively defined aftershocks.

We fit the ratio $R_\Phi(\phi) = \rho_{eq}(\phi)/\rho_{ref}(\phi)$ with a periodic function $\alpha\cos(\phi - \phi_0)$ where α quantifies the strength of the tidal modulation and ϕ_0 is the angular position of peak seismicity (Figure 2d). We fit the ratio $R_\Sigma(\sigma) = \rho_{eq}(\sigma)/\rho_{ref}(\sigma)$ with a linear function $\gamma\sigma + \beta$ where γ quantifies the tidal sensitivity of seismicity and with an exponential function derived from the rate-and-state formalism $\exp(\sigma/a\sigma_n)$ (Dieterich, 1994) where a is the rate dependence factor of rate-and-state friction and σ_n is the effective normal stress (only the product $a\sigma_n$ can be inverted for, see Figure 2h). Because of the limited range of stress amplitudes (~1 kPa), we have $\sigma/a\sigma_n \ll 1$ and

$\exp(\sigma/a\sigma_n) \approx 1 + \sigma/a\sigma_n$, implying that $\gamma \approx 1/a\sigma_n$ when the rate-and-state formula fits $R_\Sigma(\sigma)$. We choose the linear function because it is model-agnostic, easy to fit and provides a solution even when $\exp(\sigma/a\sigma_n)$ cannot fit $R_\Sigma(\sigma)$.

We computed $R_\Phi(\phi)$ and $R_\Sigma(\sigma)$ in overlapping 3.4-year windows across the 10-year catalog with 3-month steps and in a 5 km-wide box including the Ridgecrest rupture (Figure 1a). We determined time series of the parameters α, ϕ_0, γ, and ($a\sigma_n$) from the fitted models. Each sliding window looks backward so that the parameters at a given time only reflect the past. To evaluate the statistical relevance of the parameters, we built the empirical distributions of each of these parameters on permuted replica of our catalog. We divided our catalog into segments of constant earthquake numbers and produced the replica by mixing the segments (Delorey & Chen, 2022). Thus, a replica has the same number of events as the original catalog and similar inter-event times but has no dependence on the tides (see Figure S2 in Supporting Information S1). These empirical distributions were used to build the confidence intervals where the null hypothesis (seismicity and tides are independent) can be rejected.

3. Results and Tests of Robustness

The analysis of R_Φ for the Coulomb stress phase shows that, over the 10-year study period, peak seismicity occurs under favorable Coulomb stress conditions, namely when the tidal Coulomb stress or stress rate are high ($-\pi/2 \leq \phi_0 \leq 0$, Figure 3b). Before 2018, the amplitude of tidal modulation is low (Figure 3c). However, after 2018, about 1.5 years before the mainshock, we observe strong, statistically significant tidal modulation with peak seismicity aligning with peak Coulomb stress (Figure 3b). The enhanced tidal sensitivity of seismicity after 2018 is also visible with the analysis of R_Σ (Figure 3) where the slope γ is large (Figure 3e) and the product $a\sigma_n$ is low (Figure 3g), indicating that earthquakes preferentially occur under high tidal Coulomb stress at significantly higher rates than in the 9 years preceding 2018. We found a similar signal of strong tidal modulation in the analyses with tidal volumetric strain and normal stress (Figure 4). We confirmed the statistical significance of the modulation increase with the Kolmogorov-Smirnov test applied to the instantaneous phase distributions from the start and end times of the study period (Figure S4 in Supporting Information S1). Around 2016–2017, our observations suggest that peak seismicity aligns with the maximum rate of change of tidal Coulomb stress (Figure 3b) as well as that of volumetric strain (Figure 4a) and normal stress (Figure 4b). The modulation by the tidal volumetric strain and normal stress seems to increase gradually as time gets closer to the M_w 7.1 mainshock (Figure 4). We did not observe any evidence of tidal shear stress-modulated seismicity after 2018 but found significant modulation in 2016–2017, which cannot be distinguished from the modulation by volumetric strain rate and normal stress rate because both quantities are highly correlated (see Figure S5 in Supporting Information S1).

We tested the robustness of our results with respect to changes in the method parameters and possible sources of error. The choice of a single fault orientation might introduce errors in the computation of Coulomb stress on individual faults. However, our results show that volumetric strain and normal stress, and, therefore, the isotropic component of tidal stress, drive the modulation of seismicity after 2018 (Figure 4). Thus, our conclusions do not critically rely on the choice of fault orientation. It also follows that results change little when Coulomb stress is computed under different values of coefficient of friction ($\mu = 0.3, 0.6, 0.8$) except for very low values ($\mu = 0.1$) for which Coulomb stress becomes close to shear stress (Figure S6 in Supporting Information S1). To ensure that the episodes of increased seismic activity observed in September–November 2010 and May–August 2015 (see Figure 1b) were not biasing our analysis, we removed these episodes and replaced the gaps with earthquake sequences taken from times with average seismicity rates (Figure S6 in Supporting Information S1). The tidal modulation became even clearer when analyzing this modified catalog, with a more apparent gradual increase in modulation strength after 2016 (Figure S8 in Supporting Information S1). The results are also robust against changes in the window parameters used in the analysis (Figure S9 in Supporting Information S1). Varying the box width showed that narrow boxes (3, 5, and 7 km) all produced similar results but that the signal of tidal modulation started to weaken for wider boxes (10 km, see Figure S10 in Supporting Information S1). Similarly, shortening the box toward the mainshock hypocenter did not degrade the signal of enhanced tidal sensitivity after 2018. Finally, we repeated the same analysis only using earthquakes in the northernmost area of our study region (which is the most seismically active), just south of the Coso geothermal field, and used it as a control study. The results show that tidal modulation occurs throughout the study period but there is no evidence for enhanced tidal sensitivity before the M_w 7.1 Ridgecrest earthquake (Figure S11 in Supporting Information S1). These tests further show that enhanced tidal triggering prior to the mainshock occurs along the fault that ruptured during the M_w 7.1 earthquake.

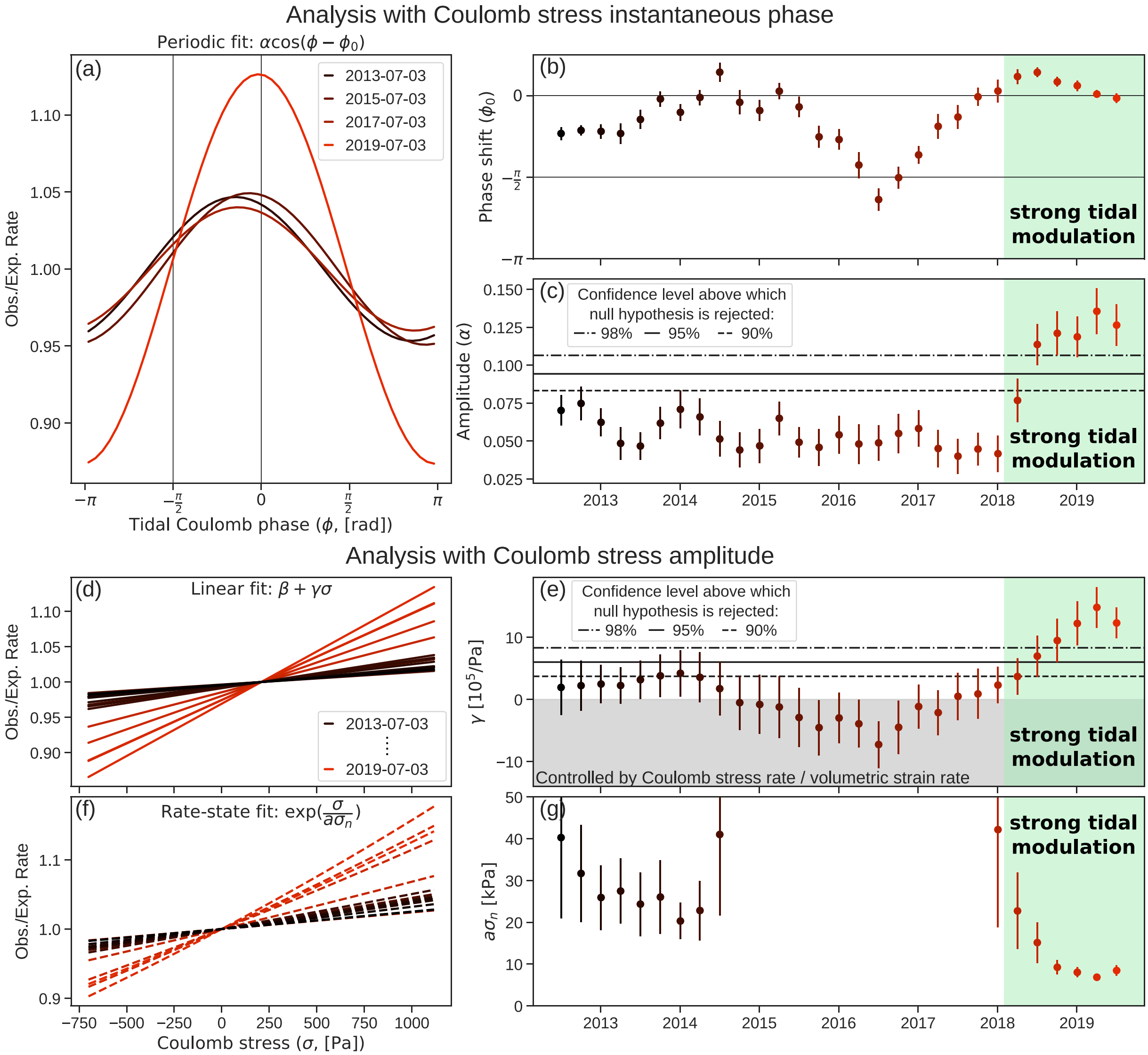

Figure 3. Analysis of tidal modulation of seismicity in terms of the instantaneous phase, ϕ (a–c), and amplitude, σ (d–g), of the tidal Coulomb stress. (a) Cosine fits $\alpha\cos(\phi - \phi_0)$ of $R_\Phi(\phi)$ for four different windows. (b) Angular position of peak seismicity, ϕ_0. The 0 radian (maximum Coulomb stress) and the $-\pi/2$ (maximum Coulomb stress rate) lines are plotted. (c) Amplitude of the cosine fit, α. In (b) and (c), the error bars are the standard deviations of 100 ϕ_0 and α estimated on perturbed R_Φ where each phase bin is randomly perturbed in proportion to its uncertainty (see Figure 2d). (d) Linear fits $\beta + \gamma\sigma$ of $R_\Sigma(\sigma)$ for all windows with positive slope γ. (e) Slope, γ, which quantifies the sensitivity of the seismicity rate to tidal stresses as a function of time. Negative slopes indicate absence of sensitivity to Coulomb stress where panel b suggests sensitivity to Coulomb stress rate. The error bars are the standard errors from the linear regression. (f) Exponential fits $\exp(\sigma/a\sigma_n)$ of $R_\Sigma(\sigma)$ for all windows with $\gamma > 0$. (g) $a\sigma_n$ product as a function of time, only for windows with $\gamma > 0$ (see panel e). The error bars are the standard deviations of 100 $a\sigma_n$ estimated on perturbed R_Σ where each stress bin is randomly perturbed in proportion to its uncertainty (see Figure 2h). In all panels, color indicates the end time of the window. In (b), (c), (e), and (g), each dot is at the end of the 3.4-year window over which the measurement was made. In c and e, horizontal lines are the 90%, 95%, and 98% confidence intervals, obtained from the permuted catalogs (Figures S2 and S3 in Supporting Information S1), above which tidal modulation is statistically significant.

4. Discussion and Concluding Remarks

Our results show that seismicity preferentially occurs at high Coulomb stress amplitudes ($\phi_0 = 0$, Figure 3b, $\gamma > 0$, Figure 3e), which is the expected behavior for oscillatory stresses with periods shorter than the earthquake nucleation time as shown in laboratory experiments with dry rock samples (Beeler & Lockner, 2003). We also see that higher seismicity is promoted by higher tidal volumetric strain and normal stress (Figure 4), implying that tidal normal stress dominates tidal Coulomb stress (high coefficient of friction, unsaturated system, Delorey & Chen, 2022).

Our observations suggest a transient departure in 2016 from the $\phi_0 = 0$ regime to the $\phi_0 = -\pi/2$ regime, where seismicity aligns with peak tidal Coulomb stress rate (Figure 3b) as well as peak volumetric strain rate and normal

10.1029/2023GL104375

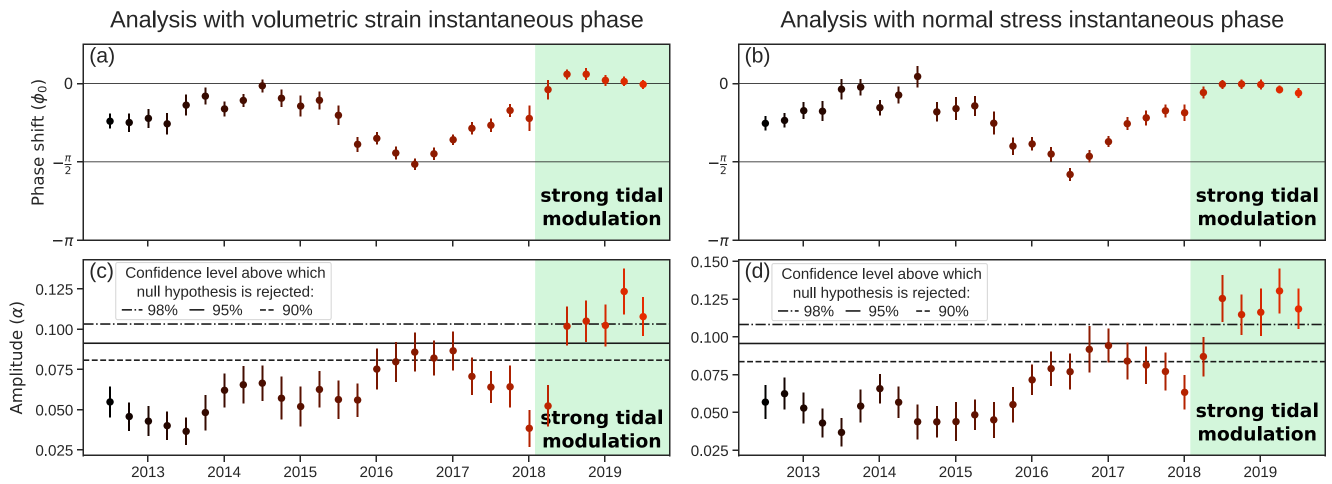

Figure 4. Analysis of tidal modulation of seismicity in terms of the instantaneous phase, ϕ, of tidal volumetric strain (a, c) and tidal normal stress (b, d). (a) Angular position of peak seismicity, ϕ_0, within the cycle of tidal volumetric strain. 0 radian is maximum (most extensive) volumetric strain and $-\pi/2$ is maximum volumetric strain rate. (b) Angular position of peak seismicity, ϕ_0, within the cycle of tidal normal stress. 0 radian is maximum (most extensive) normal stress and $-\pi/2$ is maximum normal stress rate. (c, d) Amplitude of the cosine fit, α, for tidal volumetric strain and normal stress, respectively. Horizontal lines are the 90%, 95%, and 98% confidence intervals, obtained from the permuted catalogs (Figure S2 in Supporting Information S1), above which tidal modulation is statistically significant. Error bars are the standard deviations of 100 ϕ_0 and α estimated on perturbed median ratios where each phase bin is randomly perturbed in proportion to its uncertainty (similar to Figure 2d). Each dot is at the end of the 3.4-year window over which the measurement was made.

stress rate (Figure 4), but modulation amplitudes are only between the 90% and 95% confidence levels (Figure 4), casting doubt on its physical reality. According to earthquake nucleation models, this intriguing feature would imply a significant, transient change in loading rate (Beeler & Lockner, 2003; Dieterich, 1994; Heimisson & Avouac, 2020; Pétrélis et al., 2021). However, these models do not account for poro-elastic effects; furthermore, strain rate-controlled acoustic emission activity in wet rock samples has been observed in oscillatory stress experiments (Chanard et al., 2019). They also do not account for changes in the elastic properties of the medium, although it is known that seismic velocities are modulated by the tidal volumetric strain and that largest changes occur under peak strain rate (e.g., Mao et al., 2019). Thus, both tectonic stressing and medium changes could explain this change in regime, if true. More attention should be given to this observation if confirmed in future studies.

The increased tidal modulation of seismicity after 2018 is observed in the tidal Coulomb instantaneous phase (R_Φ, Figure 3c), stress amplitude (R_Σ, Figures 3e and 3g), volumetric strain and normal stress (Figure 4) above the 98% confidence level rejecting the null hypothesis. Our results indicate that only the near-fault seismicity (Figure S10 in Supporting Information S1) shows an evolution toward enhanced tidal sensitivity prior to the M7.1 earthquake. Thus, the observed trend of increasing tidal modulation points to a relationship with the underlying earthquake preparation process. This study therefore brings a new, robust observation that corroborates the hypothesis that seismicity, especially small magnitude earthquakes, becomes more strongly modulated by tidal stresses before large ruptures (Chanard et al., 2019; Tanaka, 2010, 2012).

Models that were built within the framework of rate- and state-dependent friction (Dieterich, 1994, 2007; Heimisson & Avouac, 2020) propose that the amplitude of tidal modulation can change due to variations either in effective normal stress σ_n or in the rate-dependence factor a. Our analysis shows that the product $a\sigma_n$ decreases before the mainshock from 30 kPa at the beginning of the study to 6.5 kPa in July 2019. We note that these values are about one order of magnitude lower than those estimated in aftershock studies (Dieterich, 1994, 2007) but are similar or larger to those estimated in other tidal triggering studies (Scholz et al., 2019; Thomas et al., 2012). It is reasonable to assume the rate-dependence factor a to be constant (Delorey et al., 2017; Thomas et al., 2012) and explain the drop in $a\sigma_n$ in terms of an increase in pore-fluid pressure, although our data cannot resolve such a process. The cause for increased tidal modulation before the M_w 7.1 Ridgecrest mainshock remains elusive. Understanding it requires understanding the complex interplay between the oscillatory tidal stresses and the earthquake nucleation properties and poro-elastic response of the medium, as well as the conditions related to earthquake preparation (e.g., is the fault loading rate increasing due to deep slip?).

As data and methods keep improving, tidal analysis will play a key role in probing fault conditions and studying the earthquake preparation process. Due to methodological improvements in earthquake detection and a novel statistical analysis, we have overcome the limitations encountered in previous tidal triggering studies (Heaton, 1982; Rydelek et al., 1992; Tanaka, 2010, 2012; Vidale et al., 1998). We have corroborated the hypothesis of increased tidal modulation before large earthquakes and proposed a rigorous workflow to apply systematically to other fault systems. This work thus elevates the questions: what is the underlying connection between tidal sensitivity and fault state, and what does it imply regarding the preparation phase of large earthquakes?

Data Availability Statement

The continuous data used in this study can be downloaded from the Southern California Earthquake Data Center (https://scedc.caltech.edu/data/waveform.html). The stress state used to determine the optimally oriented fault was inferred based on focal mechanisms from Yang et al. (2012), which can be downloaded at https://scedc.caltech.edu/data/alt-2011-yang-hauksson-shearer.html. The Southern California Seismological Network (SCSN) catalog is available at https://service.scedc.caltech.edu/eq-catalogs/date_mag_loc.php (last accessed June 2023). Our earthquake catalog was built with the BackProjection and Matched-Filtering workflow (v2.0.0alpha, last accessed June 2023, https://github.com/ebeauce/Seismic_BPMF). Our earthquake catalog is available on the Zenodo platform at https://doi.org/10.5281/zenodo.8127880 (catalog v1.0.0, last accessed in July 2023).

Acknowledgments
The authors thank the editor and two reviewers for helpful comments that improved the presentation of the results and quality of the discussion. E.B. was funded by the Brinson Foundation.

References

Agnew, D. C. (2012). Spotl: Some programs for ocean-tide loading.

Beaucé, E., van der Hilst, R. D., & Campillo, M. (2022a). An iterative linear method with variable shear stress magnitudes for estimating the stress tensor from earthquake focal mechanism data: Method and examples. *Bulletin of the Seismological Society of America*, *112*(3), 1224–1239. https://doi.org/10.1785/0120210319

Beaucé, E., van der Hilst, R. D., & Campillo, M. (2022b). Microseismic constraints on the mechanical state of the North Anatolian fault zone 13 years after the 1999 M7.4 Izmit earthquake. *Journal of Geophysical Research: Solid Earth*, *127*(9), e2022JB024416. https://doi.org/10.1029/2022JB024416

Beeler, N., & Lockner, D. (2003). Why earthquakes correlate weakly with the solid Earth tides: Effects of periodic stress on the rate and probability of earthquake occurrence. *Journal of Geophysical Research*, *108*(B8), 2391. https://doi.org/10.1029/2001jb001518

Chanard, K., Nicolas, A., Hatano, T., Petrelis, F., Latour, S., Vinciguerra, S., & Schubnel, A. (2019). Sensitivity of acoustic emission triggering to small pore pressure cycling perturbations during brittle creep. *Geophysical Research Letters*, *46*(13), 7414–7423. https://doi.org/10.1029/2019gl082093

Cochran, E. S., Vidale, J. E., & Tanaka, S. (2004). Earth tides can trigger shallow thrust fault earthquakes. *Science*, *306*(5699), 1164–1166. https://doi.org/10.1126/science.1103961

Delorey, A. A., & Chen, T. (2022). Behavior of tidally triggered earthquakes depends on fluid conditions. *Bulletin of the Seismological Society of America*, *112*(6), 2890–2901. https://doi.org/10.1785/0120220036

Delorey, A. A., van der Elst, N. J., & Johnson, P. A. (2017). Tidal triggering of earthquakes suggests poroelastic behavior on the San Andreas Fault. *Earth and Planetary Science Letters*, *460*, 164–170. https://doi.org/10.1016/j.epsl.2016.12.014

Dieterich, J. (1994). A constitutive law for rate of earthquake production and its application to earthquake clustering. *Journal of Geophysical Research*, *99*(B2), 2601–2618. https://doi.org/10.1029/93jb02581

Dieterich, J. (2007). Applications of rate-and state-dependent friction to models of fault slip and earthquake occurrence. *Earthquake seismology*, *4*, 107–129. https://doi.org/10.1016/B978-044452748-6/00065-1

Heaton, T. H. (1982). Tidal triggering of earthquakes. *Bulletin of the Seismological Society of America*, *72*(6A), 2181–2200. https://doi.org/10.1785/bssa07206a2181

Heimisson, E. R., & Avouac, J.-P. (2020). Analytical prediction of seismicity rate due to tides and other oscillating stresses. *Geophysical Research Letters*, *47*(23), e2020GL090827. https://doi.org/10.1029/2020gl090827

Mao, S., Campillo, M., van Der Hilst, R. D., Brenguier, F., Stehly, L., & Hillers, G. (2019). High temporal resolution monitoring of small variations in crustal strain by dense seismic arrays. *Geophysical Research Letters*, *46*(1), 128–137. https://doi.org/10.1029/2018gl079944

Métivier, L., de Viron, O., Conrad, C. P., Renault, S., Diament, M., & Patau, G. (2009). Evidence of earthquake triggering by the solid Earth tides. *Earth and Planetary Science Letters*, *278*(3–4), 370–375. https://doi.org/10.1016/j.epsl.2008.12.024

Mousavi, S. M., Ellsworth, W. L., Zhu, W., Chuang, L. Y., & Beroza, G. C. (2020). Earthquake transformer—An attentive deep-learning model for simultaneous earthquake detection and phase picking. *Nature Communications*, *11*(1), 3952. https://doi.org/10.1038/s41467-020-17591-w

Pétrélis, F., Chanard, K., Schubnel, A., & Hatano, T. (2021). Earthquake sensitivity to tides and seasons: Theoretical studies. *Journal of Statistical Mechanics: Theory and Experiment*, *2021*(2), 023404. https://doi.org/10.1088/1742-5468/abda29

Rydelek, P. A., Sacks, I. S., & Scarpa, R. (1992). On tidal triggering of earthquakes at Campi Flegrei, Italy. *Geophysical Journal International*, *109*(1), 125–137. https://doi.org/10.1111/j.1365-246x.1992.tb00083.x

Scholz, C. H., Tan, Y. J., & Albino, F. (2019). The mechanism of tidal triggering of earthquakes at mid-ocean ridges. *Nature Communications*, *10*(1), 1–7. https://doi.org/10.1038/s41467-019-10605-2

Schuster, A. (1897). On lunar and solar periodicities of earthquakes. *Proceedings of the Royal Society of London*, *61*(369–377), 455–465. https://doi.org/10.1038/056321a0

Tan, Y. J., Waldhauser, F., Tolstoy, M., & Wilcock, W. S. (2019). Axial seamount: Periodic tidal loading reveals stress dependence of the earthquake size distribution (b value). *Earth and Planetary Science Letters*, *512*, 39–45. https://doi.org/10.1016/j.epsl.2019.01.047

Tanaka, S. (2010). Tidal triggering of earthquakes precursory to the recent Sumatra megathrust earthquakes of 26 December 2004 (M_w 9.0), 28 March 2005 (M_w 8.6), and 12 September 2007 (M_w 8.5). *Geophysical Research Letters*, *37*(2), L02301. https://doi.org/10.1029/2009gl041581

Tanaka, S. (2012). Tidal triggering of earthquakes prior to the 2011 Tohoku-Oki earthquake (M_w 9.1). *Geophysical Research Letters*, *39*(7), 35–42. https://doi.org/10.1029/2012gl051179

Thomas, A., Bürgmann, R., Shelly, D. R., Beeler, N. M., & Rudolph, M. (2012). Tidal triggering of low frequency earthquakes near Parkfield, California: Implications for fault mechanics within the brittle-ductile transition. *Journal of Geophysical Research*, *117*(B5), 5301. https://doi.org/10.1029/2011jb009036

Vidale, J. E., Agnew, D. C., Johnston, M. J., & Oppenheimer, D. H. (1998). Absence of earthquake correlation with Earth tides: An indication of high preseismic fault stress rate. *Journal of Geophysical Research*, *103*(B10), 24567–24572. https://doi.org/10.1029/98jb00594

Wang, W., & Shearer, P. (2015). No clear evidence for localized tidal periodicities in earthquakes in the central Japan region. *Journal of Geophysical Research: Solid Earth*, *120*(9), 6317–6328. https://doi.org/10.1002/2015jb011937

Yang, W., Hauksson, E., & Shearer, P. M. (2012). Computing a large refined catalog of focal mechanisms for southern California (1981–2010): Temporal stability of the style of faulting. *Bulletin of the Seismological Society of America*, *102*(3), 1179–1194. https://doi.org/10.1785/0120110311

Zhu, W., & Beroza, G. C. (2019). Phasenet: A deep-neural-network-based seismic arrival-time picking method. *Geophysical Journal International*, *216*(1), 261–273. https://doi.org/10.1093/gji/ggy423